AFRL-RZ-WP-TP-2012-0150

EFFECTS OF NANOSCALE DEFECTS ON CRITICAL CURRENT DENSITY OF $(Y_{1-x}Eu_x)Ba_2Cu_3O_{7-\delta}$ THIN FILMS (POSTPRINT)

R. Goswami, G. Spanos, and R.L. Holtz

U.S. Naval Research Laboratory

T.J. Haugan and P.N. Barnes

Mechanical Energy Conversion Branch
Energy/Power/Thermal Division

FEBRUARY 2012

AIR FORCE RESEARCH LABORATORY
PROPULSION DIRECTORATE
WRIGHT-PATTERSON AIR FORCE BASE, OH 45433-7251
AIR FORCE MATERIEL COMMAND
UNITED STATES AIR FORCE

REPORT DOCUMENTATION PAGE

1. REPORT DATE *(DD-MM-YY)*	2. REPORT TYPE	3. DATES COVERED *(From - To)*
February 2012	Journal Article Postprint	03 May 2008 – 03 May 2010

4. TITLE AND SUBTITLE

EFFECTS OF NANOSCALE DEFECTS ON CRITICAL CURRENT DENSITY OF $(Y_{1-x}Eu_x)Ba_2Cu_3O_{7-\delta}$ THIN FILMS (POSTPRINT)

5a. CONTRACT NUMBER
In-house

5b. GRANT NUMBER

5c. PROGRAM ELEMENT NUMBER
62203F

6. AUTHOR(S)

R. Goswami, G. Spanos, and R.L. Holtz (U.S. Naval Research Laboratory)
T.J. Haugan and P.N. Barnes (AFRL/RZPG)

5d. PROJECT NUMBER
3145

5e. TASK NUMBER
32

5f. WORK UNIT NUMBER
314532ZE

7. PERFORMING ORGANIZATION NAME(S) AND ADDRESS(ES)

U.S. Naval Research Laboratory
Washington, DC 20375

Mechanical Energy Conversion Branch (AFRL/RZPG)
Energy/Power/Thermal Division
Air Force Research Laboratory, Propulsion Directorate
Wright-Patterson Air Force Base, OH 45433-7251
Air Force Materiel Command, United States Air Force

8. PERFORMING ORGANIZATION REPORT NUMBER
AFRL-RZ-WP-TP-2012-0150

9. SPONSORING/MONITORING AGENCY NAME(S) AND ADDRESS(ES)

Air Force Research Laboratory
Propulsion Directorate
Wright-Patterson Air Force Base, OH 45433-7251
Air Force Materiel Command
United States Air Force

10. SPONSORING/MONITORING AGENCY ACRONYM(S)
AFRL/RZPG

11. SPONSORING/MONITORING AGENCY REPORT NUMBER(S)
AFRL-RZ-WP-TP-2012-0150

12. DISTRIBUTION/AVAILABILITY STATEMENT
Approved for public release; distribution unlimited.

13. SUPPLEMENTARY NOTES
Journal article published in *Physica C,* Vol. 470, 2010. © 2010 Elsevier B.V.

The U.S. Government is joint author of the work and has the right to use, modify, reproduce, release, perform, display, or disclose the work.

PA Case Number: NRL 09-1226-0931; Clearance Date: 03 May 2010.

14. ABSTRACT
In pulsed laser deposition of $YBa_2Cu_3O_{7-\delta}$ films, defect introduction into the films tends to anisotropically improve the pinning along the $H\|c$ direction due to the columnar growth mode of the process. In Eu-substituted samples, however, even though an increase in critical current density (J_c) in the $H\|c$ direction was observed for low fields ($H = 0.2$ T), the improvement was more notable for the $H\|ab$-plane at both low and higher fields. Herein we present detailed TEM microstructural studies to understand these new trends in $J_c(H)$, which are markedly different than flux pinning increases achieved with other methods, for example, with nanoparticle additions. Threading dislocations, observed in the Eu-substituted samples along the c-axis, account for J_c enhancement with $H\|c$ at low field. The enhanced ab-planar pinning in the Eu-substituted samples is attributed to the extensive bending of the {0 0 1} lattice planes throughout the film, and the crystal lattice defects with excess Cu–O planes, that were effective in increasing the J_c for $H\|ab$ at both low and high fields.

15. SUBJECT TERMS
laser, samples, pulsed, deposition, film, lattice, planes, nanoparticle, low field, microstructural, flux, threading, pinning, planar

16. SECURITY CLASSIFICATION OF:

a. REPORT	b. ABSTRACT	c. THIS PAGE
Unclassified	Unclassified	Unclassified

17. LIMITATION OF ABSTRACT:
SAR

18. NUMBER OF PAGES
12

19a. NAME OF RESPONSIBLE PERSON (Monitor)
Timothy J. Haugan

19b. TELEPHONE NUMBER *(Include Area Code)*
N/A

Effects of nanoscale defects on critical current density of $(Y_{1-x}Eu_x)Ba_2Cu_3O_{7-\delta}$ thin films

R. Goswami [a,b,*], T.J. Haugan [c], P.N. Barnes [c], G. Spanos [a], R.L. Holtz [a]

[a] US Naval Research Laboratory, Washington, DC 20375, United States
[b] Science Applications International Corporation (SAIC), Washington, DC 20375, United States
[c] Air Force Research Laboratory, Wright-Patterson Air Force Base, OH 45433, United States

ABSTRACT

In pulsed laser deposition of $YBa_2Cu_3O_{7-\delta}$ films, defect introduction into the films tends to anisotropically improve the pinning along the $H||c$ direction due to the columnar growth mode of the process. In Eu-substituted samples, however, even though an increase in critical current density (J_c) in the $H||c$ direction was observed for low fields ($H = 0.2$ T), the improvement was more notable for the $H||ab$-plane at both low and higher fields. Herein we present detailed TEM microstructural studies to understand these new trends in $J_c(H)$, which are markedly different than flux pinning increases achieved with other methods, for example, with nanoparticle additions. Threading dislocations, observed in the Eu-substituted samples along the c-axis, account for J_c enhancement with $H||c$ at low field. The enhanced ab-planar pinning in the Eu-substituted samples is attributed to the extensive bending of the {0 0 1} lattice planes throughout the film, and the crystal lattice defects with excess Cu–O planes, that were effective in increasing the J_c for $H||ab$ at both low and high fields.

© 2010 Elsevier B.V. All rights reserved.

1. Introduction

The inclusion of lattice defect structures in high temperature superconducting (HTS) $REBa_2Cu_3O_{7-\delta}$ (REBCO or REBCO) thin films (RE = rare-earth element) offers great promise for increasing the in-field critical current density (J_c). This is particularly important for power applications such as generators or motors, operating at 77 K [1]. Enhancement of the flux pinning has previously been obtained with partial substitution of the lighter RE atoms, such as Nd, Sm and Eu [2–5], into sintered powders of $Re_{0.2}Y_{0.8}Ba_2Cu_3O_{7-y}$. More recent studies have demonstrated that significant increases also can be achieved in REBCO films with the addition of nanoparticles, second-phase materials [4–7], or by variable temperature processing [8], in addition to processing of mixed (RE_1,RE_2)BCO compositions [9]. In the absence of nanoscale second phase inclusions, other induced microstructural defects and sources of lattice distortions can provide pinning [10].

Although these pinning phenomena significantly increase the $J_c(H)$ of the compound, typically the enhancement is anisotropic and dependent on the particular growth mode of the deposition process. For example, in pulsed laser deposited (PLD) films, stacking faults have been shown to enhance J_c more so when the applied field (H) is parallel to the c-axis direction, due to the effect on columnar growth of the process [11]. In Metal-Organic Deposition (MOD) processed films, on the other hand, the laminar growth preferentially enhances the J_c for the magnetic field applied parallel to the ab-plane, and not the c-axis field orientation [12]. For power applications, such as motors and generators, it is important that flux pinning is sufficient in both the c-axis and ab-planar directions [13].

It is critical to understand how various types of defects can supply the pinning force in both directions, particularly in the non-preferred growth mode direction. The present investigation provides an understanding of how this was accomplished in PLD $(Y_{1-x}Eu_x)Ba_2Cu_3O_{7-\delta}$ thin films (with x ranging from 0.0 to 0.5) on CeO_2 buffered $(Zr,Y)O_2$ substrates. Thin films of $(Y_{1-x}Eu_x)$BCO ($x = 0-1$) were studied recently by several groups, and distinct differences of $J_c(H,\theta)$ were observed for these films when compared to YBCO [14,15]. However, microstructural defects of the (Y,Eu)BCO films were not examined closely by TEM yet, and the defects that caused the J_c differences were only suggested [14,15]. Herein, microstructural defects on the nanometer scale were studied by TEM, and were identified to correlate with enhanced J_c in the planar direction.

2. Experimental details

Thin films of $(Y_{1-x}Eu_x)Ba_2Cu_3O_{7-\delta}$ with $x = 0$, 0.3 and 0.5 were deposited by pulsed laser deposition (PLD) on CeO_2-buffer-coated

* Corresponding author. Address: US Naval Research Laboratory, Washington, DC 20375, United States. Tel.: +1 202 767 1676.
   E-mail address: ramasis.goswami@nrl.navy.mil (R. Goswami).

(Zr,Y)O$_2$ substrates at the rate of 10–20 nm/min with a substrate temperature of 775 °C. Details of the processing conditions and reasons for this substrate choice were given elsewhere [14]. A post-deposition anneal was performed at 500 °C and 1 atmosphere of O$_2$ for 30 min, followed by a cool down in pure O$_2$ to <60 °C in about 30 min. Transport J_c measurements (J_{ct}) were made with the four-probe method, and using a criterion of 1 μv/cm [14]. The films were patterned into microbridges typically 0.05 cm wide by 0.3 cm long, using UV laser etching with a ceramic mask. The standard error of J_{ct} measurements was not worse than 5%, and generally better than 2% [14]. Angular $J_c(H,\theta)$ measurements were made with $J \perp H$, (maximum Lorentz force configuration). Transmission electron microscopy (TEM), fine probe energy dispersive spectroscopy (EDS) and high angle annular dark-field (HAADF) imaging were employed to characterize the microstructure, using a Philips-CM 30 and JEOL-2200 microscopes. Cross-section TEM samples were prepared in a Fischione ion mill equipped with a liquid-nitrogen cold trap, using a gun voltage of 5 kV, a current of 5 mA, and an incident angle of 12°.

3. Results and discussion

The dependence of J_c on applied magnetic fields was measured by transport methods for (Y,Eu)BCO films, as shown in Fig. 1. The trends of J_c(77 K, $H \| c$) were consistent for a range of Eu substitu-

tion (Eu = 0.3–0.5); i.e. J_c significantly increased compared to YBCO for $H \| c < 1$ T, and decreased for $H \| c > 1$ T. These trends interestingly were greatest for the largest Eu substitution, Eu = 0.5. These results were not a consequence of simply changing the substrate from LaAlO$_3$ to CeO$_2$-buffer-YSZ, since YBCO samples with both substrates show the same behaviors [14]. The trends shown in Fig. 1 also were confirmed with an even larger number of films, for J_c measured by magnetic methods and published elsewhere [14]. The decreases for $H > 1$ T are in contrast atypical compared to films processed with nanoparticle additions, where large increases of J_c (77 K, $H > 1$ T) were observed [4,6]. With increasing Eu substitution, J_c(77 K, $H > 1$ T) is consistently decreased, suggesting that correlated defects parallel to c-axis were decreased by some mechanism. The increase of J_c at the lower fields ($H < 1$ T) is greater with Eu substitution than with nanoparticle additions [4,6], and interestingly is comparable to the increase of $J_c(H < 1$ T) with additions of CeO$_2$ multilayers [5]. These behaviors all indicate that the microstructure is markedly changed in the films with Eu substitution.

The effects of Eu substitution on the angular dependence of J_c also were measured under an applied magnetic field, H_{appl}, for θ, the angle between H_{appl} and the c-axis of the film, from 0° to 90° [14]. Figs. 2a and b show the $J_c(\theta)$ for YBCO (Y$_{0.7}$Eu$_{0.3}$)BCO and (Y$_{0.5}$Eu$_{0.5}$)BCO at 77 K for H_{appl} = 0.2 T and 1 T, respectively. For H = 0.2 T, the $J_c(\theta)$ of (Y$_{0.7}$Eu$_{0.3}$)BCO and (Y$_{0.5}$Eu$_{0.5}$)BCO increased steadily with increasing θ, compared with a flatter dependence
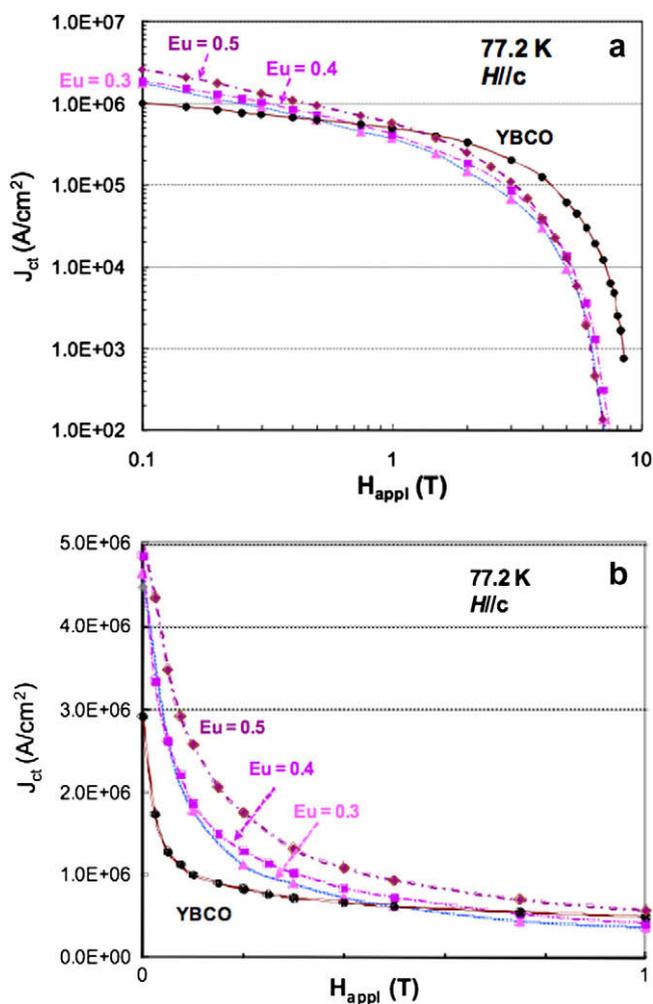
Fig. 1. Dependence of J_c on magnetic field for (Y,Eu)BCO films. (a) Up to 9 T $H \| c$ and (b) $H \| c$ less than 1 T data on a linear–linear scale.
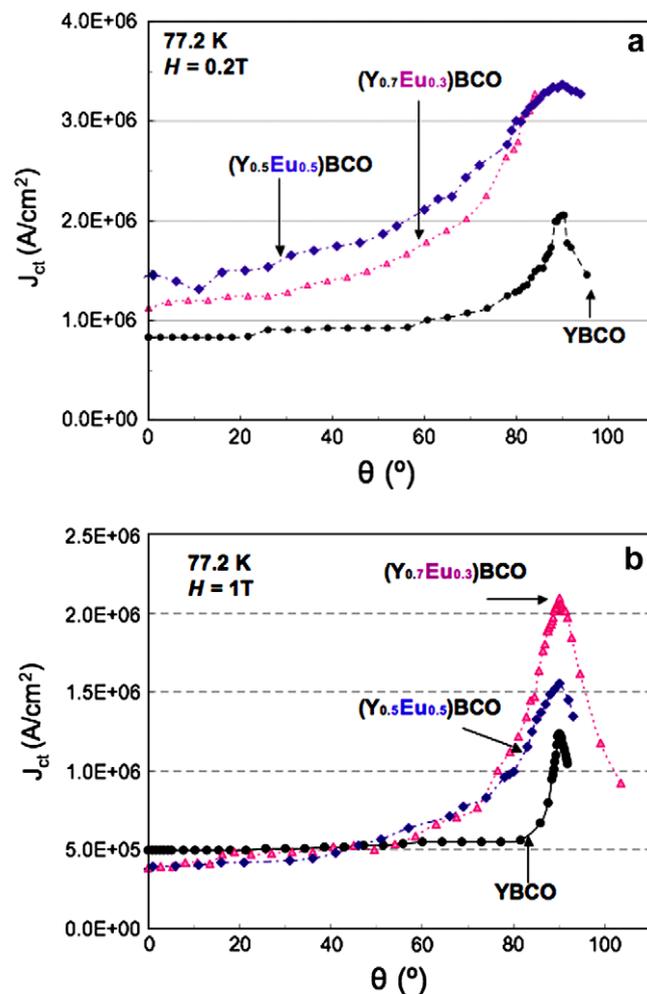
Fig. 2. Angular dependence of J_c for low and high fields for Eu substituted (Eu = 0.3, 0.5) and unsubstituted samples: (a) at 0.2 T and (b) at 1 T. θ = 90° corresponds to $H \| ab$.

on θ and a sharper *ab*-plane peak ($\theta = 90°$) for YBCO – see Fig. 2a. Specifically, at 0.2 T, for $\theta = 0$ ($H \| c$) the J_c is 1.12×10^6 A/cm^2 for (Y$_{0.7}$Eu$_{0.3}$)BCO and 1.4×10^6 A/cm^2 for (Y$_{0.5}$Eu$_{0.5}$)BCO corresponding to an increase in J_c of about 33% and 65%, respectively, as compared to the J_c of unsubstituted YBCO at 0.2 T. At a higher magnetic field, 1 T, the J_c for $\theta = 0$ ($H \| c$), *decreased* by about 10% for both (Y$_{0.7}$Eu$_{0.3}$)BCO and (Y$_{0.5}$Eu$_{0.5}$)BCO. The overall trends of J_c(77 K, θ, $H = 0.2$ and 1 T) for Eu substitution are markedly different from the unsubstituted YBCO films.

To associate the trends of $J_c(\theta, H)$ with pinning structures in the films, TEM was performed on these films specifically to determine the microstructure, defects, and compositional variations at the nano scale, as a function of Eu-substitution. In the Eu-substituted samples, the most notable features capable of accounting for sig-

nificant pinning was a high density of threading dislocations observed parallel to the *c*-axis, and extending from close to the substrate–film interface up to the film surface (Fig. 3a). These threading dislocations tend to be associated with dislocation half loops close to the CeO$_2$/(Y$_{1-x}$Eu$_x$)BCO ($x = 0.3$ and 0.5) interface. Some dislocations apparently nucleated very close to the planar defects away from the interface, and ended at planar faults, as shown in Fig. 3a and b. The number density and average spacing of the observed threading dislocations was $\sim 40 \times 10^{12}$ m^{-2} and ~ 100 nm, respectively. The matching field for this density is well below 1 T, consistent with the loss of *c*-axis pinning in the 1 T field and for $H > 1$ T [14]. Typically, a distortion zone approximately 6–8 nm in diameter and running parallel to the threading dislocations was observed (Fig. 3b). The formation mechanism of such threading dislocations, usually introduced in the early stages of growth at the substrate/film interface, is related to the growth and coalescence of YBa$_2$Cu$_3$O$_{7-\delta}$ islands [16,17].

Although threading dislocations have been observed in PLD grown unsubstituted YBCO by other authors [16,18], the current cross-sectional TEM observations showed no threading dislocations in the unsubstituted YBCO films on CeO$_2$-buffer-(Y,Zr)O$_2$ substrates in the present study. This could be due to the relatively higher deposition temperatures or longer post annealing treatment [16], which can decrease the dislocation density to a significant extent. Alternatively, the high density of pores observed in the unsubstituted YBCO films in this study, ranging from 100 to 200 nm in size, with a number density of 2×10^{12} m^{-2}, could have suppressed the formation of extended threading dislocations by relieving residual stress in the trenches of the growth islands to a significant extent. On the other hand, a considerable *decrease* in the density of pores, down to 1×10^{11} m^{-2}, was observed in the Eu-substituted samples, which conversely showed a high density of threading dislocations. The high density of *c*-axis correlated threading dislocations/defects ($\sim 40 \times 10^{12}$ defects m^{-2}) that form in the Eu-substituted films would be expected to provide strong pinning centers, and thus contribute to flux pinning at low fields [16,18], as demonstrated in Fig. 2a.

For H parallel or nearly parallel to the *ab*-plane ($75° \leqslant \theta \leqslant 90°$), both low ($H = 0.2$ T) and high ($H > 0.2$ T) fields resulted in a very large increase of J_c for the Eu-substituted ($x = 0.3$) film compared to the unsubstituted ($x = 0$) film, as observed in Fig. 2. The J_c values for $H \| ab$ for the Eu-substituted films and the unsubstituted YBCO film at 0.2 T are $\sim 3.5 \times 10^6$ A/cm^2 and 2×10^6 A/cm^2, respectively, indicating an increase in J_c by a factor of 1.75 T (see Fig. 2a). At $H \| ab = 1$T, J_c increases by a factor of 1.25–1.6 due to the different levels of Eu-substitution (see Fig. 2b). The types of defects that enhance J_c for $H \| ab$ correspond to strong *ab*-planar pinning rather
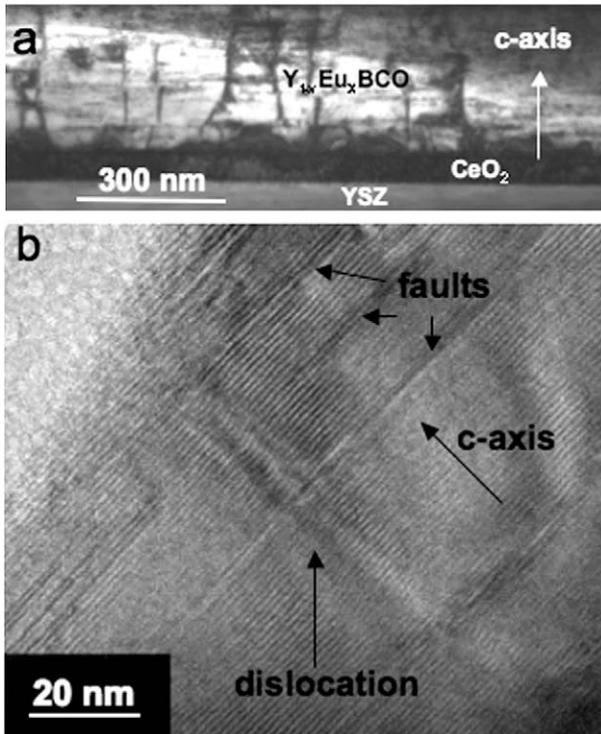
Fig. 3. (a) A bright-field cross-sectional TEM image of the Eu-substituted ($x = 0.3$) sample showing a high density of threading dislocations. The dislocation lines are almost parallel to the *c*-axis. (b) A HRTEM image showing the distortion around a threading dislocation and very fine planar faults.
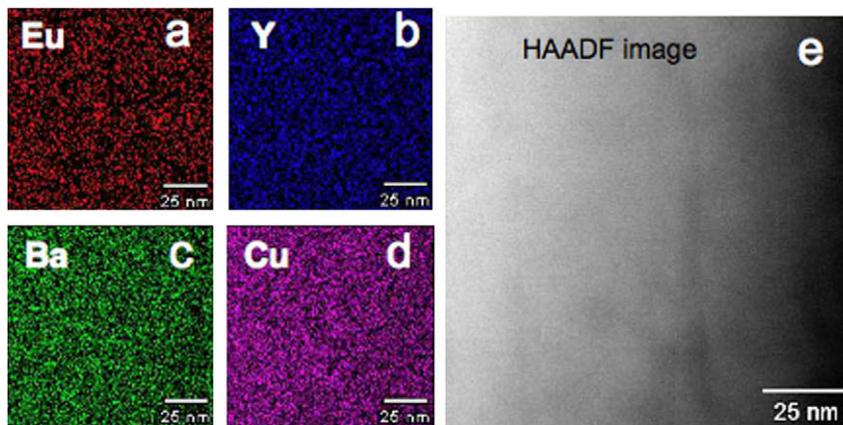
Fig. 4. (a–d) The fine probe EDS showing the distribution of Eu, Y, Ba and Cu. (e) The corresponding HAADF image of the film with Eu = 0.3.
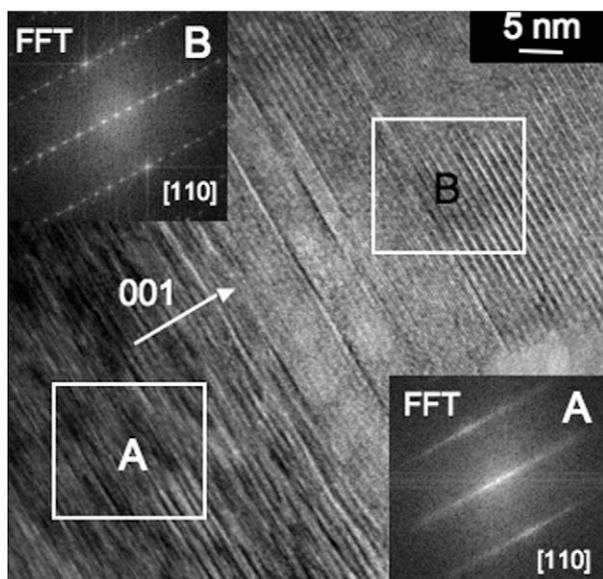
Fig. 5. HRTEM image of the unsubstituted sample close to the [1 1 0] zone showing lattice bending and the high density faults close to the interface. Fast Fourier transforms (FFTs) from regions marked as "A" and "B" are shown as insets. Note that the lattice bending away from the CeO$_2$/YBCO interface (see the region around B in the image) has decreased considerably.

than *c*-axis correlation, even though columnar PLD growth generally enhances defect propagation in the *c*-axis direction. The angular dependence of J_c in the Eu-substituted samples for H nearly parallel to the *ab*-plane ($75° \leqslant \theta \leqslant 90°$) is considerably broad at the low as well as the high field. This indicates enhanced correlated and random pinning in the *ab*-plane introduced by the Eu substitution [15]. In X-ray diffraction (XRD) the (0 0 5) peak of the Eu-substituted samples were predominantly single, which indicates that bimodal distributions of EuBCO and YBCO unit cells did not exist, at least in agglomerations large enough such that the unit cells could be distinguished and measured by XRD. The fine scale distribution of Eu, Y, Ba and Cu was obtained by the fine probe EDS with a probe size of 0.5 nm in Eu-substituted samples. It was observed that they were uniformly distributed in the film (Fig. 4), which corroborate the XRD observations.

In order to elucidate the type of defect structure correlated with the *ab* pinning in these materials, microstructures of both unsubstituted and Eu-substituted samples were considered in more detail. Fig. 5 is a high-resolution TEM image of the unsubstituted YBa$_2$Cu$_3$O$_{7-\delta}$(YBCO), showing higher density of faults and considerable lattice buckling close to the CeO$_2$/YBCO interface. The corresponding fast Fourier transform (FFT) from the region "A" close to the CeO$_2$/YBCO interface showed considerable angular spread of {0 0 *l*} type of planes. Continuous streaks also observed along the YBCO [0 0 1] direction in the fast Fourier transform (FFT) are due to the presence of very thin faults (1–3 nm thick) lying in the (0 0 1) plane, as verified by the fact that the streaks are perpendicular to the thin dimension of the faults. TEM observations also revealed that the lattice buckling and the density of faults substantially decreased away from the interface, for the unsubstituted sample (see Fig. 5 close to region B and above). The fast Fourier transform (FFT) from the region "B" away from the CeO$_2$/YBCO interface showed sharp spots of {0 0 *l*} type of reflections, indicating no lattice buckling.

In the Eu-substituted samples, however, the lattice buckling (Fig. 6) as well as fine faults (Fig. 3b) was present throughout the film. Note such lattice buckling in unsubstituted films was observed close to the CeO$_2$/YBCO interface. The lattice buckling of {0 0 *l*} type of plane can be clearly observed in the inverse-Fourier
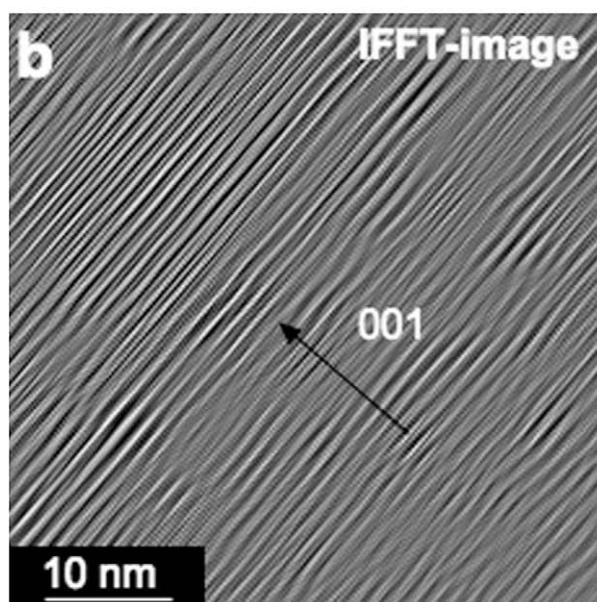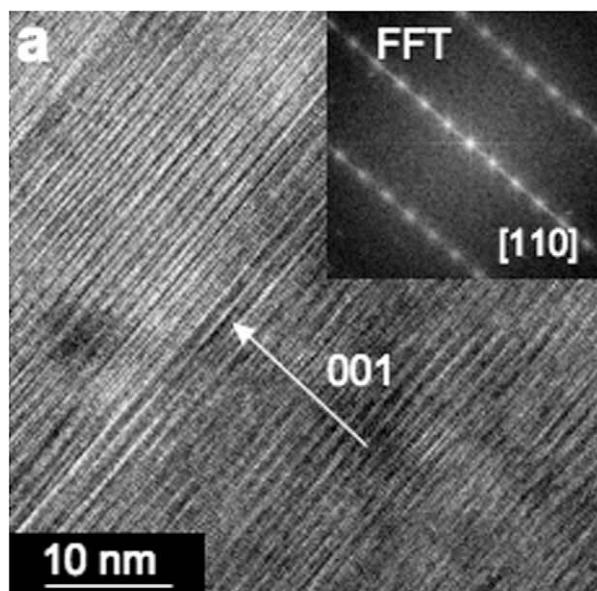
Fig. 6. (a) A HRTEM image close to the [1 1 0] zone showing the lattice bending of (0 0 1) planes in the Eu-substituted (*x* = 0.3) sample. The FFT is shown in the inset. (b) The corresponding IFFT-image showing the lattice bending throughout the entire region.

transform (IFFT) image (Fig. 6b) of the Eu-substituted film (*x* = 0.3). Another observation was the presence of other type of defect, in the Eu-substituted films, which had extra *c*-axis faults lying in the *a*–*b* plane. Fig. 7a is a HRTEM image of the Eu-substituted film (*x* = 0.3) showing the presence of double oxide layers with a spacing between the layers of ∼0.37 nm. The corresponding inverse-Fourier transform image (IFFT) given in Fig. 7b clearly shows the double oxide layers. Normally strong white fringes of Cu–O planes between the Ba–O planes are observed at ≈1.2 nm spacing for YBCO [19]. Such double strong white fringes with similar intensities observed in the (Y$_{0.7}$Eu$_{0.3}$)BCO films indicate the presence of excess Cu-oxide layers.

Similar growth conditions were used for unsubstituted and Eu-substituted films. TEM results showed, in addition to typical stacking faults which are present in both unsubstituted and substituted samples with similar density, extensive buckling of {0 0 *l*} type of plane (*a*–*b* plane) throughout the film and the *ab*-planar-type defects with double Cu–O planes. These will enhance flux pinning

4
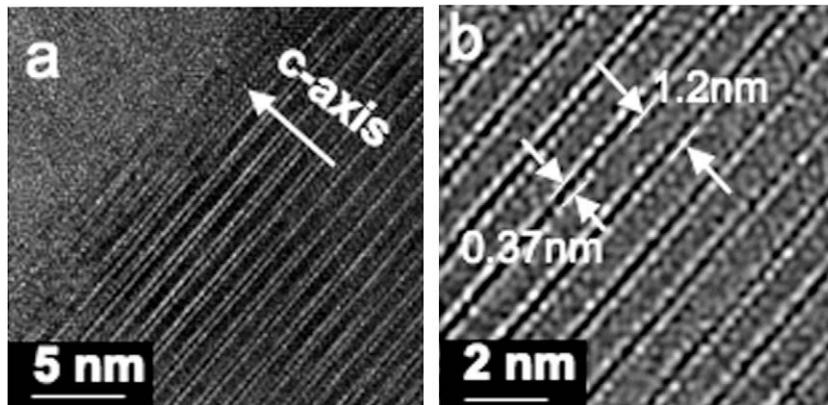
Fig. 7. (a) HRTEM image showing the excess Cu–O planes in $(Y_{0.7}Eu_{0.3})BCO$. (b) The corresponding inverse FFT (IFFT) image also shows the double Cu–O planes.

considerably in the a–b plane as compared to the unsubstituted film, and thus would account for the continued enhancement of J_c for $H||ab$ at both low and high fields.

4. Summary

In summary, the microstructure and defects of $(Y_{1-x}Eu_x)Ba_2Cu_3O_{7-\delta}$ thin films samples with different levels of Eu, produced by the pulsed laser deposition (PLD) process, have been studied by transmission electron microscopy techniques. A considerable increase in J_c (30–65%) for $H||c = 0.2$ T was observed in the Eu-substituted $x = 0.3$, 0.5 samples, compared to the J_c of unsubstituted $YBa_2Cu_3O_{7-\delta}$. Also, for $H||ab$ and/or H near the ab-plane ($75° \leqslant \theta \leqslant 90°$), a significant increase of J_c was observed for both $x = 0.3$ and 0.5 Eu-substituted films (compared to the unsubstituted film), for both low and high fields ($H \geqslant 0.2$ T). It was shown that threading dislocations along the c-axis can account for the increase of J_c for $H||c$ ($\theta = 0$) at low field. Additionally for Eu-substituted films, extensive buckling of the $\{0\,0\,l\}$ type lattice planes throughout the film, and the ab-planar-type defects with double Cu–O planes will enhance flux pinning considerably in the a–b plane as compared to the unsubstituted film, and thus would account for the continued enhancement of J_c for $H||ab$ at both low and high fields.

Acknowledgements

References

[1] D. Larbalestier, A. Gurevich, D.M. Feldmann, A. Polyanski, Nature 414 (2001) 368.
[2] Y. Li, Z.X. Zhao, Physica C 351 (2001) 1.
[3] Y. Li, N. Chen, Z. Zhao, Physica C 221 (1994) 391.
[4] T. Haugan, P.N. Barnes, R. Wheeler, F. Meisenkothen, M. Sumption, Nature 430 (2004) 867.
[5] P.N. Barnes, T.J. Haugan, C.V. Varanasi, T.A. Campbell, Appl. Phys. Lett. 85 (2004) 4088.
[6] J.L. MacManus-Driscoll, S.R. Foltyn, Q.X. Jia, H. Wang, A. Serquis, L. Civale, B. Maiorov, M.E. Hawley, M.P. Maley, D.E. Peterson, Nat. Mater. 3 (2004) 439.
[7] R. Goswami, R.L. Holtz, M.W. Rupich, W. Zhang, G. Spanos, Acta Mater. 55 (2007) 6746.
[8] Y. Yoshida, Y. Ichino, M. Miura, Y. Takai, K. Matsumoto, A. Ichinose, S. Horii, M. Mukaida, IEEE Trans. Appl. Supercond. 15 (2005) 2727.
[9] J.L. MacManus-Driscoll et al., Appl. Phys. Lett. 86 (2005) 032505.
[10] T. Matsushita, Supercond. Sci. Technol. 13 (2000) 730.
[11] J. Wang, J.H. Kwon, J. Yoon, H. Wang, T.J. Haugan, F.J. Baca, N.A. Pierce, P.N. Barnes, Appl. Phys. Lett. 92 (2008) 082507.
[12] E.D. Specht, A. Goyal, J. Li, P.M. Martin, X. Li, M.W. Rupich, Appl. Phys. Lett. 89 (2006) 162510.
[13] P.N. Barnes, M.D. Sumption, G.L. Rhoads, Cryogenics 45 (2005) 670.
[14] T.J. Haugan, T.A. Campbell, N.A. Pierce, I. Maartense, P.N. Barnes, Supercond. Sci. Technol. 21 (2008) 025014.
[15] H. Zhou, B. Maiorov, H. Wang, J.L. MacManus-Driscoll, T.G. Holesinger, L. Civale, Q.X. Jia, S.R. Foltyn, Supercond. Sci. Technol. 21 (2008) 1.
[16] J.M. Huijbregtse, B. Dam, R.C.F. van deer Geest, F.C. Klaassen, R. Elberse, J.H. Rector, R. Griessen, Phys. Rev. B 62 (2000) 1338.
[17] S.J. Pennycook, M.F. Chisholm, D.E. Jesson, R. Feenstra, S. Zhu, X.Y. Zheng, D.J. Lowndes, Physica C 202 (1992) 1.
[18] B. Dam et al., Nature 399 (1999) 439.
[19] A.F. Marshall, R.W. Barton, K. Char, A. Kapitulnik, B. Oh, R.H. Hammond, S.S. Laderman, Phys. Rev. B 37 (1988) 9353.